Rapp. P.-v. Réun. Cons. int. Explor. Mer, 180: 83–92. 1982.

# An explicit numerical model to simulate upwelling events

C. Brockmann

Deutsches Hydrographisches Institut
Bernhard-Nocht-Strasse 78, 2000 Hamburg 4, Bundesrepublik Deutschland

E. Maier-Reimer and H. Meier-Fritsch

Max Planck Institut für Meteorologie
Bundesstrasse 13, 2000 Hamburg 13, Bundesrepublik Deutschland

A three-dimensional numerical model for upwelling has been developed and tested under various boundary conditions. Gridsize and bottom topography are variable; the driving force is windstress. A version of the model was applied to data from the "Upwelling 75" experiment. Certain wind-induced events observed in the data are reproduced reasonably well, although wind input is done by means of linear approximation. Typical upwelling conditions can be achieved and the influence of bottom topography can be shown.

## Introduction

It was assumed that data sets available off the Northwest African coast could be interpreted and understood by a numerical model. Since upwelling must be considered as a three-dimensional process off West Africa, a new model has been developed. Distinct from Hurlburt (1974), O'Brien and Hurlburt (1972), and Thompson (1974), the vertical component of the velocity field is calculated from the law of conservation. The convective terms of density transports are also taken into account. The aims are a better understanding of the sensitivity of the model, and application to field data. To date the model has been applied to field data from the "Upwelling 75" experiment. The oceanographic work is described by Anon. (1977) and Brockmann et al. (1977). The positions of current meter moorings used for comparison are shown in Figure 60.

## Model

The model is based on the Navier-Stokes equations, the law of conservation, and a density-advection equation. Hydrostatic approximation is used. The set of equations is given in the Appendix. The model is three dimensional with respect to space, and has relative bottom topography. The grid resolution in space is a compromise between different requirements. In the region of the actual upwelling, the resolution could not be coarser than 5 nm. Owing to the limited capacity of the computer available, only a rather small area could be covered by such a fine grid. The solution would then be completely determined by the boundary conditions, which should be prescribed despite the fact that they are unknown.

Therefore, in our model, the grid increment increases with the distance from the upwelling region. With this layout, the grid covers the whole North Atlantic up to the Americas, where plausible boundary conditions can be given. The differential equations are solved by an explicit difference scheme first set up by Maier-Reimer (unpublished). As initial state, a uniformly stratified fluid at rest was assumed. The driving force is windstress. Boundary conditions are tested for the bottom (slip and non-slip conditions); for the walls non-slip is used. In the model layout, all the features and advantages of numerical upwelling models described in the résumé given by O'Brien et al. (1977) are included. However, a disadvantage arose: when dealing with surface waves, the Courant-Friedrich-Levy criterion requires time steps not greater than 20 seconds with the chosen grid configuration. So four different versions of this surface boundary condition have been tested.

Using the complete condition

$$w_s = \frac{\partial \zeta}{\partial t} + u \frac{\partial \zeta}{\partial x} + v \frac{\partial \zeta}{\partial y}$$

compared with the linearized

$$w_s = \frac{\partial \zeta}{\partial t}$$

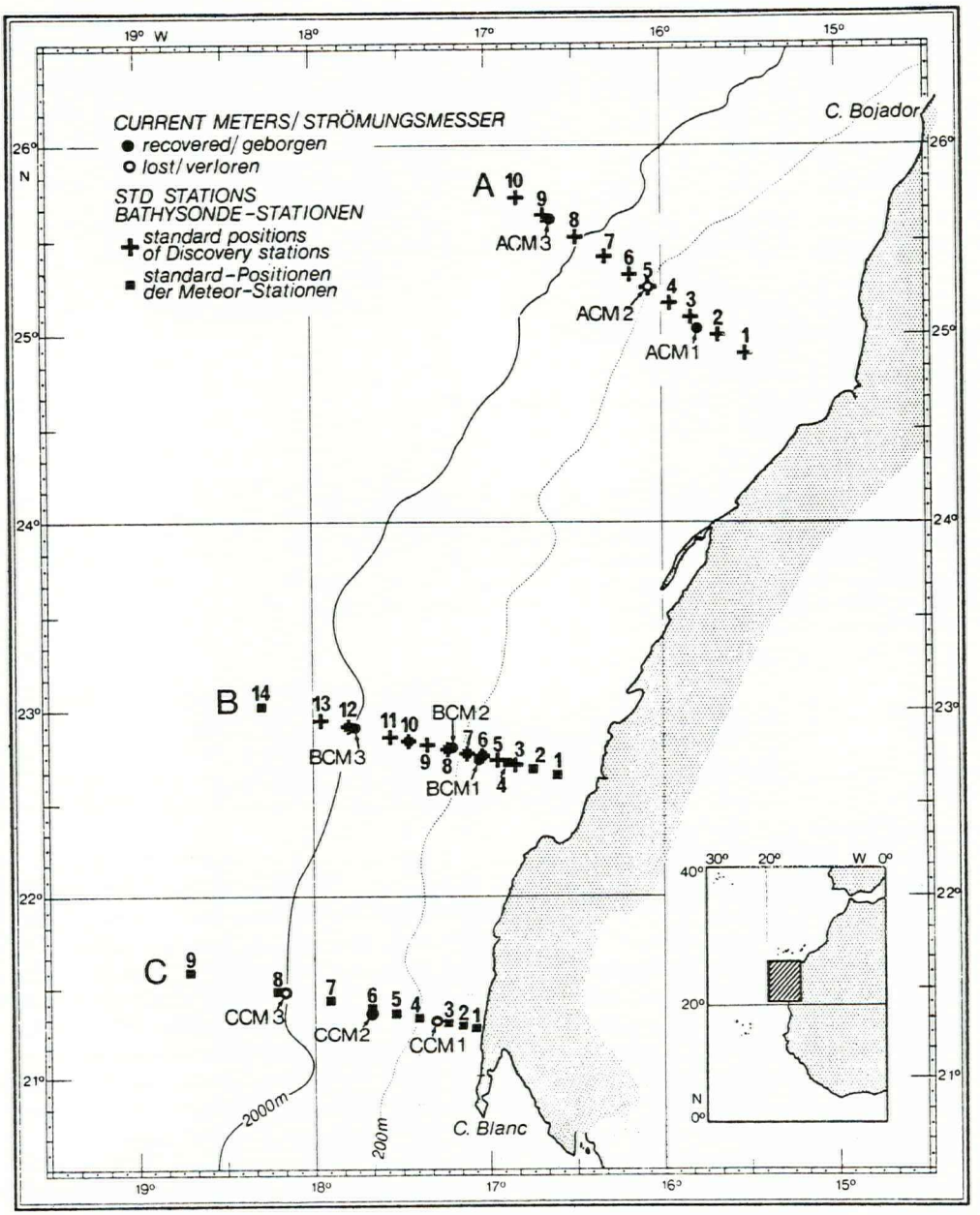


Figure 60. Current meter moorings and standard STD stations of "Upwelling 75".

results in only very small differences (less than 0·01 cm for water displacement and less than 0·001 cm/s for velocity). As upwelling is a baroclinic phenomenon, it is advantageous to filter out barotropic waves responsible for the strong limitations of the time step. Sugihara (1977) and others have successfully used the so-called rigid-lid approximation by simply neglecting the water elevation

$$w_s = \frac{\partial \zeta}{\partial t} = 0.$$

By means of the condition

$$w_s = \frac{\partial \zeta}{\partial t} * \text{const.}$$

with a constant of 100, one obtains stable results. With this semi-flexible "rubber" surface, the change of surface elevation with respect to time is assumed to be 1/100th of the vertical component in the uppermost grid points. This boundary condition filters out the short-period surface waves, and attenuates those with

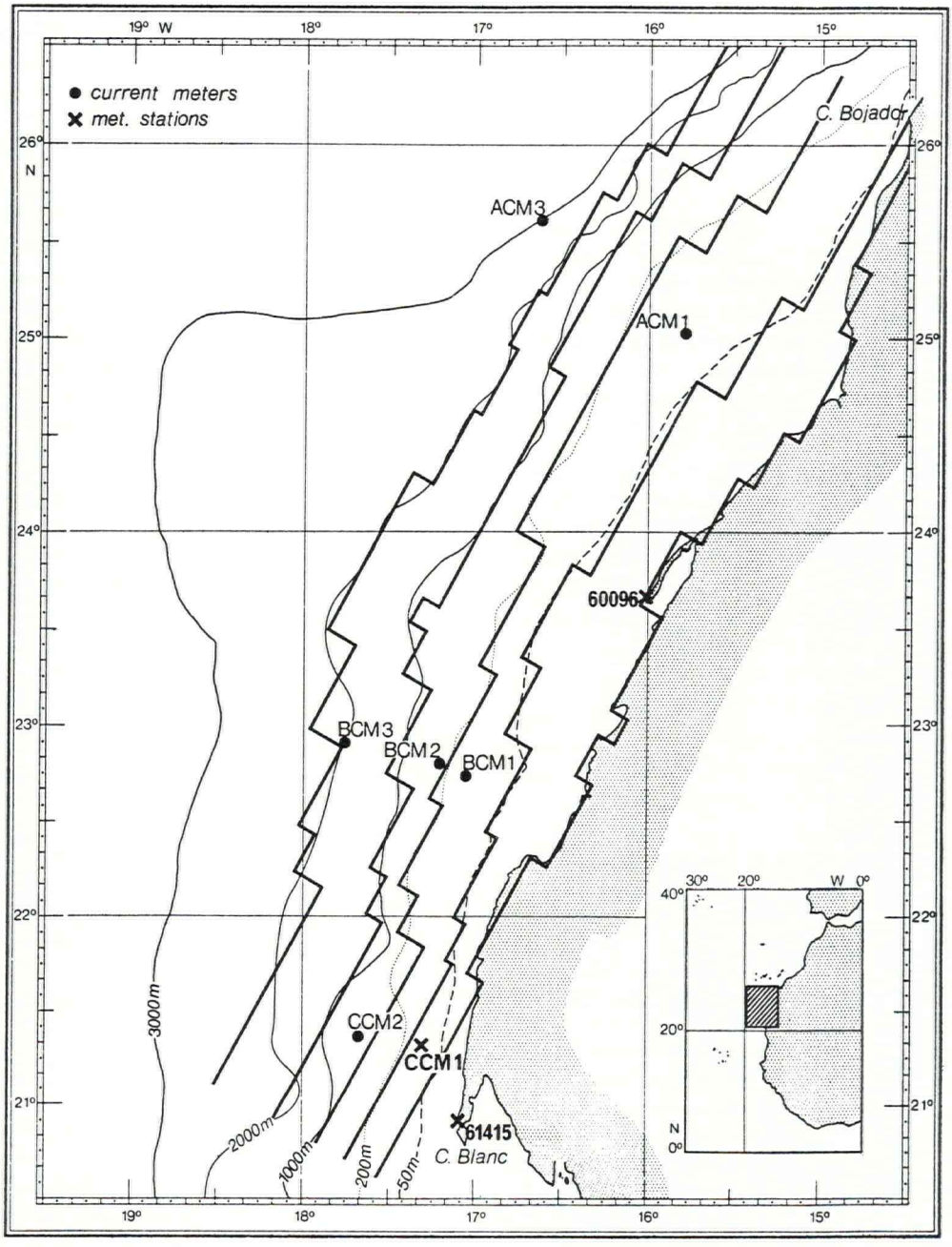


Figure 61. Bottom topography model/actual.

longer periods, which enables the time step to be increased to 300 seconds. With the help of this damping the condition of the sea surface is allowed to adjust smoothly to the changing wind field, the values of which are known only every six hours according to the abundance of the experimental data.

Spin-up is performed by means of linearly increasing windstress for the various test cases. North and east wind conditions were investigated for a 14-day period. A test area with bottom topography like that during the 1977 upwelling experiment was used. While the north wind solution yields to the typical upwelling situation on the shelf, as observed in the field experiment, the east wind solution shows a longshore component towards north. The current on the shelf is considerably stronger with the north wind. The density gradients on

the shelf normal to the coast are much sharper with the east wind. A small isolated region of downwelling appears at the same position under both north and east winds. This seems to be an effect of the local topography.

A detailed discussion of various boundary conditions and an application of this model to the "Auftrieb 77" data are in preparation (Meier-Fritsch, 1979).

The results show the typical upwelling scales, as given by Smith (1968). A small version of the model, using non-slip conditions at bottom and walls as well as variable bottom topography, has been used for application to the data set of the "Upwelling 75" field experiment. The bottom topography is shown in Figure 61. For part of the study a constant vertical austausch coefficient of 100 g/cm/s and a horizontal, grid-dependent one of $O(10^7)$ g/cm/s has been used. Although the results are encouraging, a problem arises from the large amount of cpu-time needed.

Three of the surface boundary conditions were used with a so-called "real wind field" (see next section) for the first two and a half months of 1975: 1) a rigid-lid surface, time step 300 s, 2) a "rubber" surface, time step 300 s, 3) a free surface, time step 20 s, used as comparison for a restricted time only.

## Wind field

The 1975 experiment did not lead to a sufficient set of wind data for use in a numerical model. Since the model spin-up takes place from the initial state of no motion, it was important to find a set of wind data for all grid points, with time series starting long before the experimental data set. Since the time-series data from the meteorological instruments on the moorings were of poor quality and the use of ship's data would have meant integrating measurements from variable positions, no attempt was made to use real data in constructing the wind field for the model.

The best input data would come from a meteorological mesoscale model, but so far, only wind data from synoptic stations are available. There are five stations surrounding the test area:

1) WMO/OMM station 60030 Las Palmas in the north,
2) WMO/OMM station 60096 Villa Cisneros (northeast edge of the inner grid),
3) WMO/OMM station 61415 Nouadhibou (southeast edge of the inner grid),
4) WMO/OMM station 8583 Mindelo (Cape Verde Islands; in the south),
5) WMO/OMM station 8594 Sal (Cape Verde Islands; in the south).

The available data on wind speed and direction have a time interval of six hours. All gaps were removed by interpolation using splines on the components. Measurements from 1 January to 15 March 1975 were used. From these data windstress in longshore and offshore components was calculated using the formula

$$\tau_i = \varrho \cdot c \cdot |\vec{v}_i| \cdot \vec{v}_i; \qquad c = 1{\cdot}6\times10^{-3};$$
$$\varrho = 1{\cdot}225\times10^{-3}\ \mathrm{g/cm^3}; \qquad i = 1,2.$$

The assumption of a drag coefficient $c$ of $1{\cdot}6\times10^{-3}$ was made according to Wucknitz et al. (1975) and Bush (1973). To calculate windstress for each gridpoint, the assumption was made that longshore and offshore changes in the windfield were small enough to allow linear approximation in each component. This was done by means of a least-square fit for each component. As a result inaccuracies arose immediately in the input data; there was an error due to the deflecting influence of the islands. In addition a more crucial error was caused by neglecting the nonlinear terms. However, owing to the fact that the components were treated separately, a rotation in the windfield was still possible. Furthermore, owing to the linear approach the sea breeze had an effect far offshore. Since Clancy's results (1975) show an amplifying influence of the sea breeze, it was not filtered out.

Figure 62 shows some of the wind time series. A) is an unfiltered time series, clearly showing the daily variations of the sea breeze. B) is a time series calculated with the above-mentioned linear approximation. C) and D) are filtered time series from the two coastal stations, which are quite different in magnitude and slightly different in direction, possibly due to local influences. E) is the filtered input into the model at the position of mooring B3, still reproducing the "major" features visible in both of the measured time series. In this sense "major" features are the prevailing direction and fluctuations in amplitude, taking place several times during the observation and calculation period. Three events were accentuated: About 15 February, a period with strong winds parallel to the coast could be observed. On 24 February, a decrease followed by rapid increase took place. On 28 February, the wind turned onshore and decreased again. Local effects cannot be reproduced by the linear attempt made. This is seen in Figure 63, which shows the spatial wind distribution on 25 February 1975, and the time series of the wind measurements at position B1 (Fig. 64, top). For this reason, the 1975 measurements have been checked for time series which have good correlation with the wind field available. Only stations B1 and B2 seem to be comparable with the input used.

Further difficulties arise from the fact that the model uses a closed basin. To avoid boundary problems, and to reproduce natural phenomena as far as model limitations allow, the wind was turned more to the west and reduced over the southern points. Towards the western

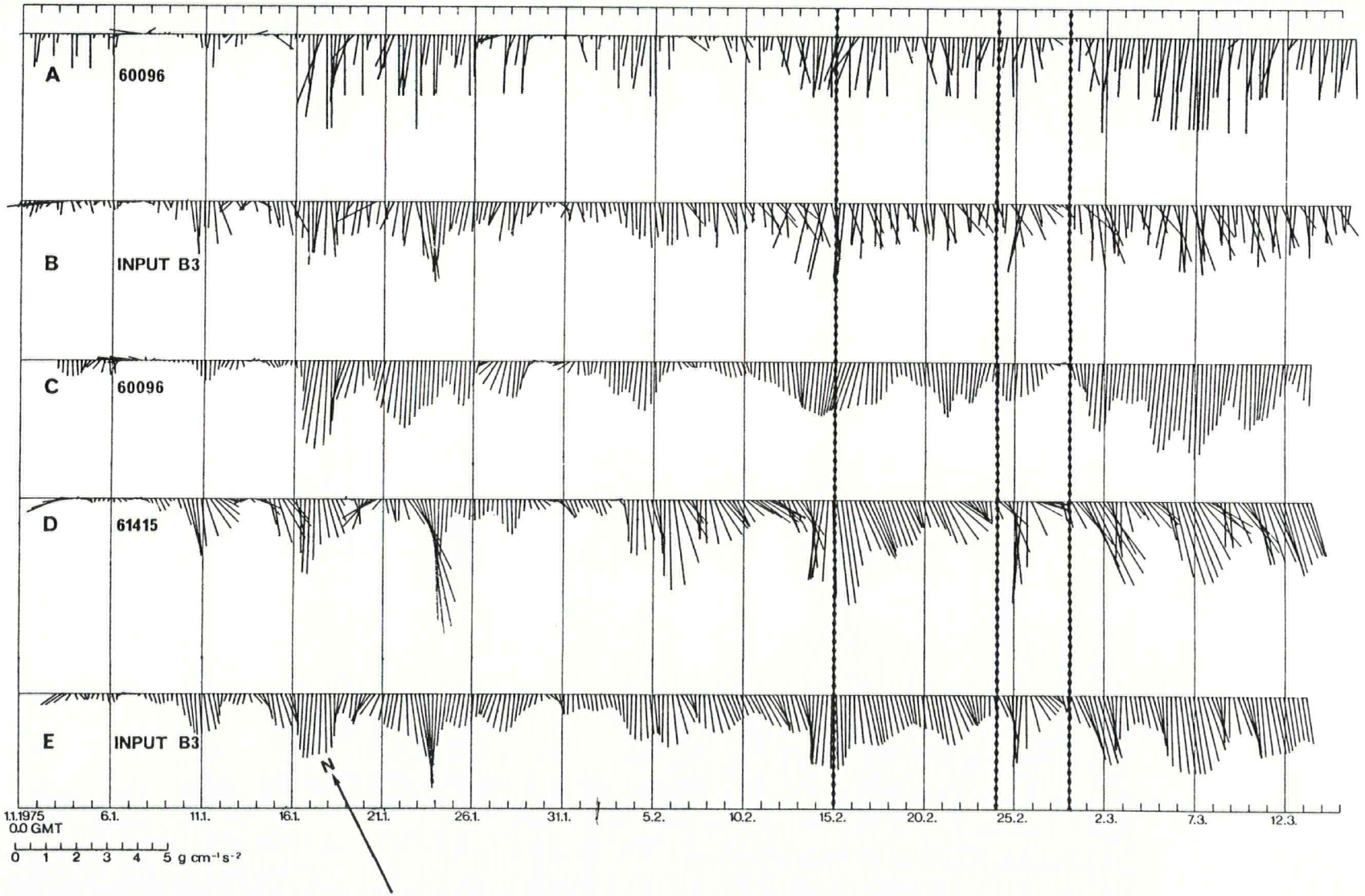


Figure 62. Wind time series. A) Measured values WMO/OMM station. B) Model input at mooring position. C) Measured values WMO/OMM station, filtered. D) Measured values WMO/OMM station, filtered. E) Model input at mooring position, filtered.

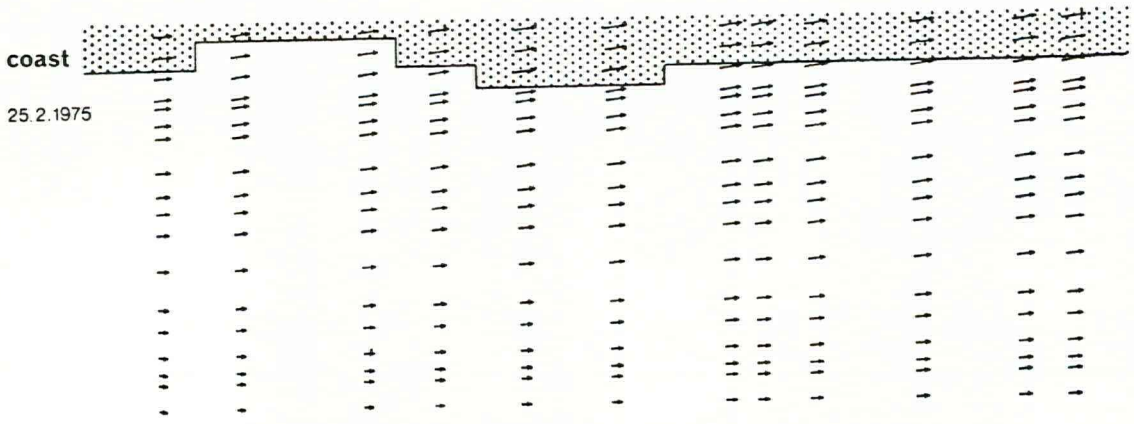


Figure 63. Spatial wind distribution, (25 February 1975), computed.

boundaries, the wind was reduced as well. Spin-up was caused by a linearly increasing windstress over 3000 time steps up to the value for 1 January 1975 for each gridpoint. For the calculation itself, the values between the six-hourly input data were also linearly interpolated.

## Results

Corresponding to the restrictions of the model only the main features of the 1975 events can be expected to be reproduced. Furthermore, simplifications in bottom

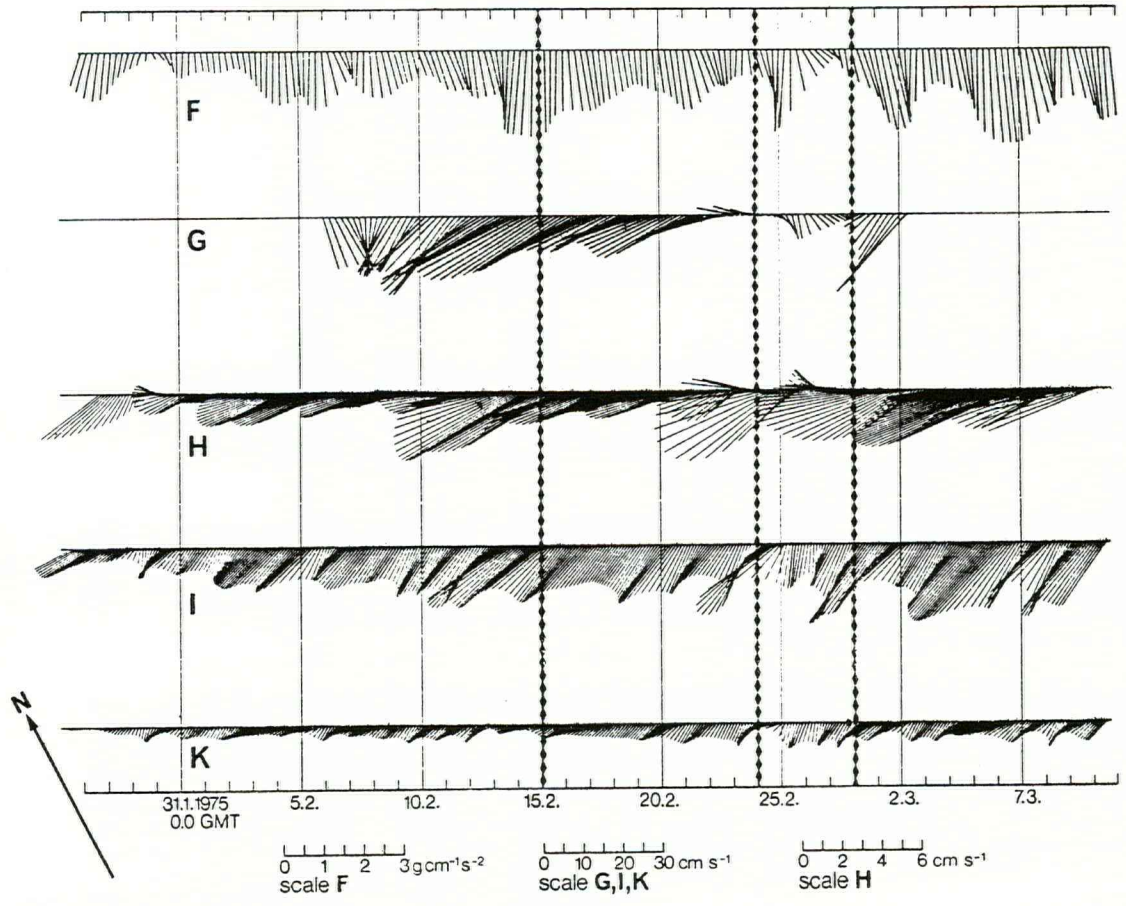


Figure 64. Model results (filtered) at mooring position B1. F) Wind input. G) Measured values (30 m). H) "Rigid-lid"-model results (10 m). I) "Rubber-lid"-model results (20 m). K) "Rubber-lid"-model results (40 m).

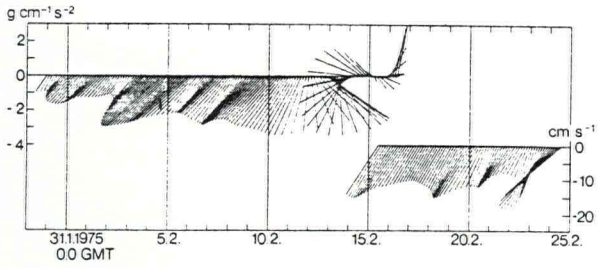


Figure 65. Filtered wind time series at mooring position C1 (top). Free surface model results at 30 m (bottom).

topography make it difficult to find corresponding places to compare with the 1975 moorings. Beyond this, the inner grid area is too small to reproduce typical mesoscale effects of this area, such as the geostrophic gyre described by Fedoseev (1970). At this stage of investigation, moorings B1 and B2 are considered to be positions where the model should have some relation to reality. Figure 64 shows stick-plots of: F) filtered wind input (F-K are filtered with 32 h half-power point, 60 weights), G) measured time series, H) results from the model with rigid lid, I), K) results from

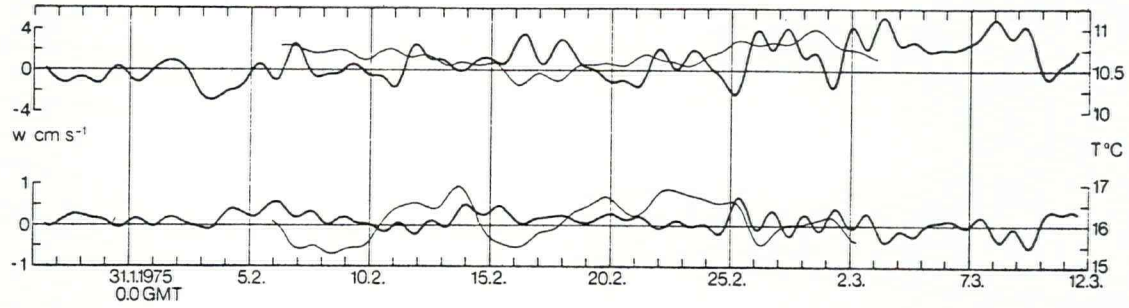


Figure 66. Computed vertical velocity (thick lines) versus measured temperature (thin lines). Velocity scaled with factor $10^3$.

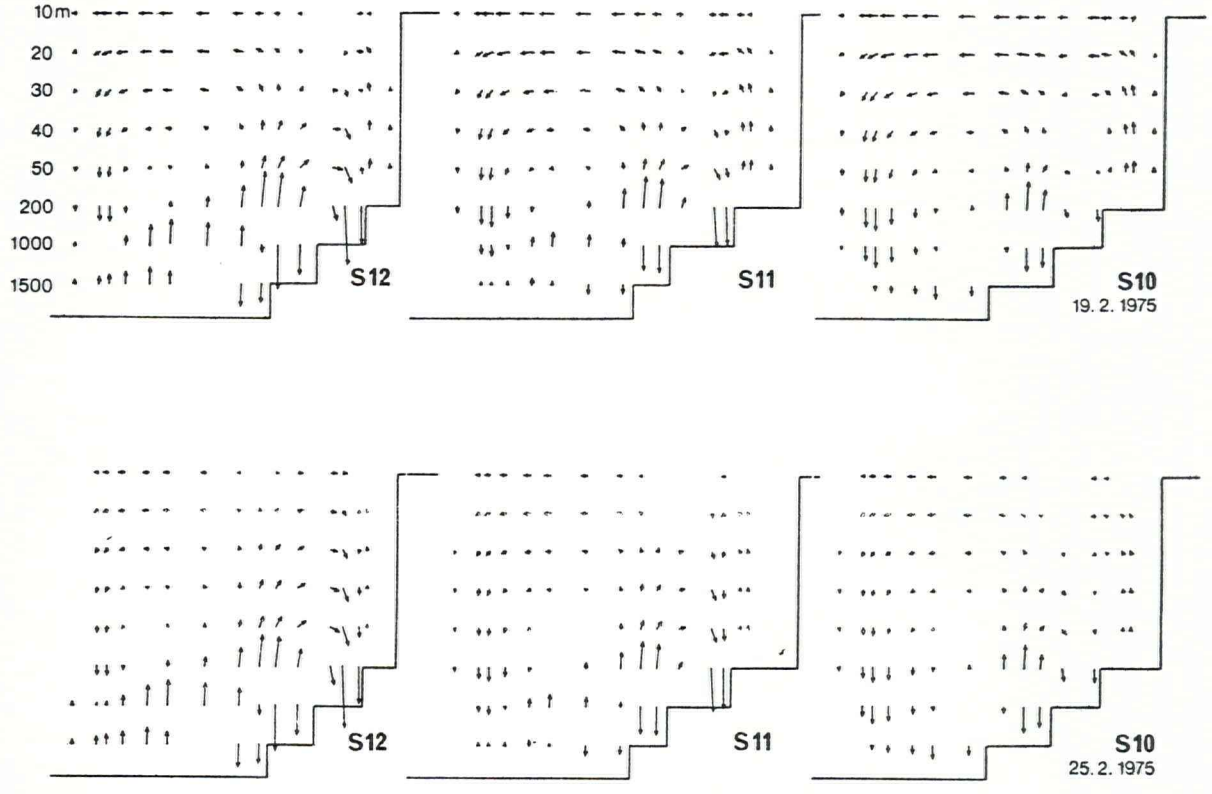


Figure 67. Offshore sections at gridpoints on line B (S11), one grid distance south (S12) and north (S10). Vertical velocities scaled with factor $10^3$.

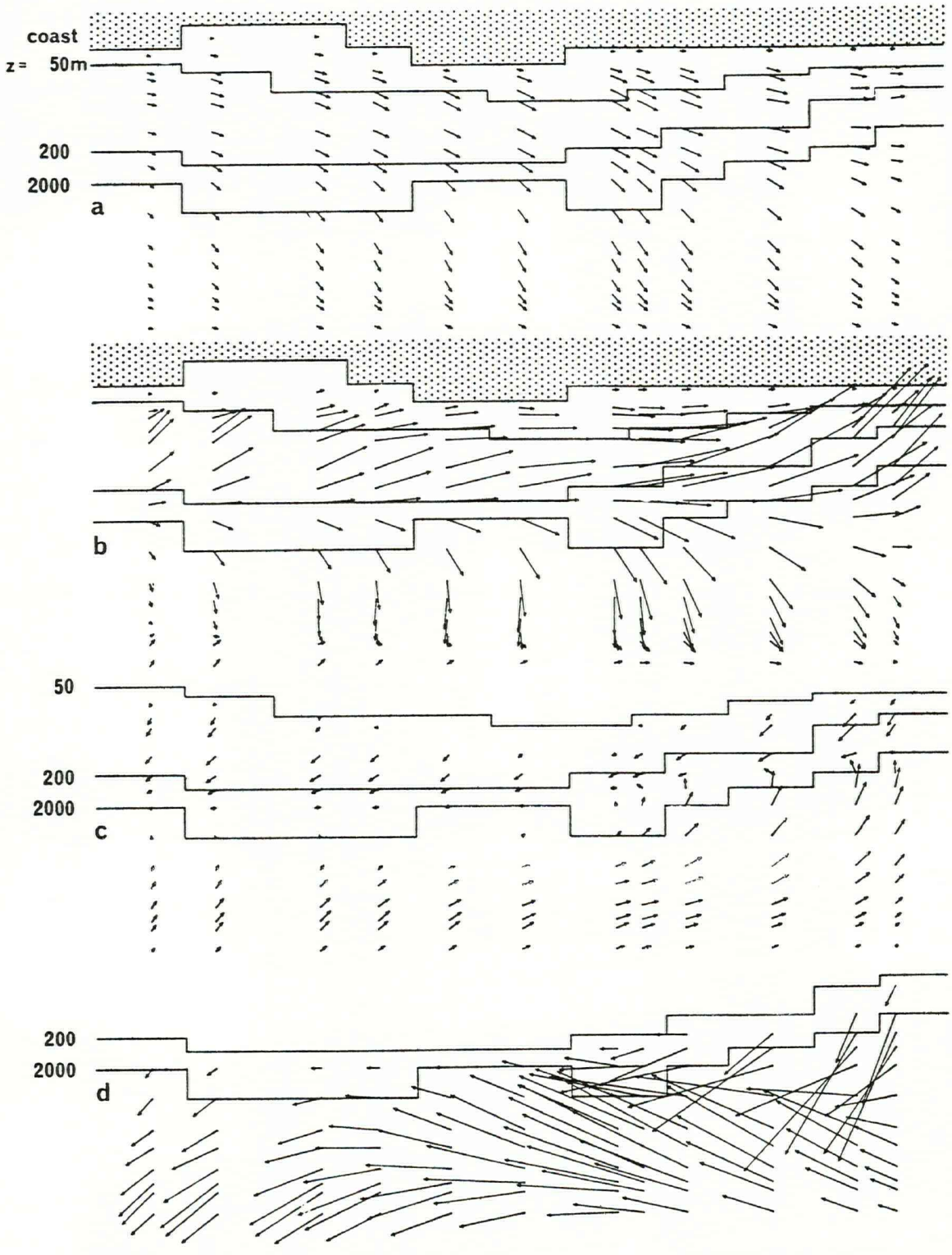


Figure 68. Horizontal current distribution at various depths (arbitrary scales, 19 February 1975, at a) 10 m, b) 40 m, c) 200 m, d) 1500 m).

the model with semi-flexible lid below. Figure 65 shows the results of the free surface model for a period of a few days. Not taking into account that all velocities are too low (which will be discussed later), there seem to be – to a certain extent – some similarities with the measurements.

As the model output of a $u$ (longshore) and $v$ (offshore) is calculated at discrete points (~ 5 km apart), there might be a better correlation with the observed data by interpolating to the same point, which was not done for the stick-plots shown. All marked events, as registrations of mooring B1 show, are wind induced. The results of the rigid-lid model show a clearly inertia-governed regime. The results of "rubber" and "free" models are quite similar. This comes up to expectations, as the input wind field has time intervals of six hours (= 1080 time steps, free surface model, = 72 time steps, "rubber" surface), which allows the surface to react in time in both models. Besides the visible correspondence of some events, Figure 65 (top) shows the lack of wind input in the model. The measured winds at mooring C turn through 180° on 15 February 1975, which cannot be observed in the input used. Despite the model's limitations and the assumptions made, Figure 66 is encouraging. The thin lines are measured temperatures while the thick ones are computed vertical velocities – showing that the model has some positive qualities. The wind-driven upwelling events are reproduced quite well. Figure 67 shows instantaneous sections with a two-cell circulation, as observed by many authors (e.g., Mittelstaedt, 1976) and computed by others (e.g., Thompson, 1974). Finally, Figure 68 once more points out the importance of bottom topography.

## Future application

The linear construction of the windfield may be one reason for the difference in magnitude of computed and observed current speed. In addition there are the constant vertical diffusion and the horizontal diffusion of $O(10^7)$. The missing history of the current field (prior to 1 January 1975) also has to be taken into account. Thus there are several possible effects which, if incorporated, would allow the model to give more realistic velocity values.

The crucial weaknesses, namely, too few gridpoints and the input windfield, will be improved. As pointed out by Speth et al. (1978), West African upwelling is mainly winddriven. The data used for that study came from an analysis of surface pressure from a model with grid spacing of about 100 km belonging to the Deutsche Wetterdienst. This data will be used in the model discussed in this paper as well. Detlefsen and Speth's (1979) results on an empirical factor analysis of surface pressure gradients show that it should not be difficult to improve this model.


## Acknowledgements

We wish to express our thanks to our colleagues for their helpful ideas and suggestions. This study – as well as the 1975 and 1977 upwelling expeditions – was supported by the Deutsche Forschungsgemeinschaft.


## References


Anon. 1977. RRS "Discovery" cruise 69. Cruise report no. 51. (Unpublished manuscript).

Brockmann, C., Hughes, P., and Tomczak, M. 1977. Data report on currents, winds and stratification in the NW African upwelling region. Ber. Inst. Meeresk., 32.

Bush, N. E. 1973. The surface boundary layer. Boundary-Layer Meteorol., 4: 213–240.

Clancy, R. M. 1975. The mesoscale interaction between coastal upwelling and the seabreeze circulation. M. Sc. thesis, University of Miami.

Detlefsen, H., and Speth, P. 1979. Empirical orthogonal analysis of surface pressure gradients (in prep.).

Fedoseev, A. 1970. Geostrophic circulation of surface waters on the shelf of North-West Africa. Rapp. P.-v. Réun. Cons. int. Explor. Mer., 159: 32–37.

Hurlburt, H.-E. 1974. The influence of coastline geometry and bottom topography on the eastern ocean circulation. Florida State University. Univ. tech. Rep., 103 pp.

Meier-Fritsch, H. 1979. An explicit numerical model of upwelling. (Unpublished manuscript).

Mittelstaedt, E. 1976. On the currents along the North-West-African coast south of 22° North. Dt. hydrogr. Z., 29: 97–117.

O'Brien, J.J., and Hurlburt, H.-E. 1972. A numerical model of coastal upwelling. J. phys. Oceanogr., 2: 14–26.

O'Brien, J. J., et al. 1977. Upwelling in the ocean: Two and three-dimensional models of upper ocean dynamics and variability. *In* Modelling and prediction of the upper layers of the ocean, pp. 178–228. Ed. by E. B. Kraus. Pergamon Press, New York.

Smith, R. 1968. Upwelling. Oceanogr. Mar. Biol. Ann. Rev., 6: 11–46.

Speth, P., Detlefsen, H., and Sierts, H.-W. 1978. Meteorological influence on upwelling off Northwest Africa. Dt. hydrogr. Z., 31: 95–104.

Suginohara, N. 1977. Upwelling front and two-cell circulation. J. oceanogr. Soc. Japan, 33: 115–130.

Thompson, J. D. 1974. The coastal upwelling cycle on a β-plane: Hydrodynamics and thermodynamics. Ph. D. thesis, Florida State University.

Wucknitz, J., et al. 1975. Bulk aerodynamics description of the turbulent fluxes at the surface with and without precipitation. GATE-Report 14 (II): 262–269.


## Appendix

$$\frac{\partial u}{\partial t} + u\frac{\partial u}{\partial x} + v\frac{\partial u}{\partial y} + w\frac{\partial u}{\partial z} - fv + \frac{1}{\varrho}\frac{\partial p}{\partial x} =$$

$$\frac{\partial}{\partial x}\left(A_H\frac{\partial u}{\partial x}\right) + \frac{\partial}{\partial y}\left(A_H\frac{\partial u}{\partial y}\right) + \frac{\partial}{\partial z}\left(A_V\frac{\partial u}{\partial z}\right) + F$$

$$\frac{\partial v}{\partial t} + u\frac{\partial v}{\partial x} + v\frac{\partial v}{\partial y} + w\frac{\partial v}{\partial z} + fu + \frac{1}{\varrho}\frac{\partial p}{\partial x} =$$

$$\frac{\partial}{\partial x}\left(A_H\frac{\partial v}{\partial x}\right) + \frac{\partial}{\partial y}\left(A_H\frac{\partial v}{\partial y}\right) + \frac{\partial}{\partial z}\left(A_V\frac{\partial v}{\partial z}\right) + F$$

$$p(z) = -g\int\varrho dz$$

$$\frac{\partial u}{\partial x} + \frac{\partial v}{\partial y} + \frac{\partial w}{\partial z} = 0$$

$$\frac{\partial \varrho}{\partial t} + u\frac{\partial \varrho}{\partial x} + v\frac{\partial \varrho}{\partial y} + w\frac{\partial \varrho}{\partial z} = 0$$

$$f = 2\,\omega\sin\varphi.$$